

Stress analysis of linear elastic structures by the fast multipole boundary element method

Jacek Ptaszny and Piotr Fedeliński

Department of Strength of Materials and Computational Mechanics

Silesian University of Technology

ul. Konarskiego 18A, 44-100 Gliwice, Poland

e-mails: jacek.ptaszny@polsl.pl, piotr.fedelinski@polsl.pl

(Received in the final form January 15, 2010)

In this paper a fast multipole boundary element method (FMBEM) analysis of internal stress in two-dimensional linear elastic structures is presented. The expansions of the potentials occurring in the stress integral equation are obtained by the differentiation of local series built for the displacement equation potentials, and application of the strain-displacement and stress-strain relations. Results of the analysis are presented. To illustrate the accuracy of the method a stress concentration problems are considered, which are a square plate with a circular hole under tension, and a gear. The application of the FMBEM can reduce the analysis time in relation to the conventional BEM case, providing similar accuracy. Presented method can be applied in the BEM analysis of non-linear structures, which requires the evaluation of internal strains or stresses.

Keywords: linear elasticity, stress analysis, boundary element method, fast multipole method.

1. INTRODUCTION

The fast multipole method (FMM) by Greengard and Rokhlin [4] has been successfully applied by many authors to the boundary element method (BEM) analysis of elastic structures. The application of the method overcomes the main drawback of the BEM, namely unsymmetric and fully populated matrices of the system of equations causing at least quadratic computational complexity of the conventional BEM. The fast multipole BEM (FMBEM) does not operate implicitly with the whole matrices, but with matrix-vector products. Therefore, the complexity is reduced to the linear one for structures with a large number of degrees of freedom (DOF). Before the FMM was developed the BEM application was usually limited to the analysis of structures of at most several thousands of degrees of freedom. Presently, structures with millions of DOF can be analysed using ordinary PC desktop computers.

A number of publications concerning the FMBEM analysis of elastostatic problems can be found. A survey of the applications in the years 1996-2001 is presented in Nishimura [10]. Here a short review of articles published in the recent years will be given. Englund and Helsing [3] analysed 2-D stress problems of perforated finite domains. They applied Fredholm equation of the second kind with the use of the FMM. Results for a loaded single edge notched specimen with many holes were presented. Of, Steinbach and Wendland [11] developed a fast multipole Galerkin BEM. They applied the method in certain engineering and industrial applications, i. e. the stress analysis of a press equipment part and a metallic foam. In Yao et al. [20] an analysis of 2-D composite materials was presented. The approach of repeated subdomain was applied to the determination of effective elastic properties of solids containing many inclusions of different shapes. Structures with the ideal interface between the matrix and inclusions, and with interlayers were analysed. Wang and Yao [17] developed a version of the FMBEM with additional exponential expansions of the kernels and

their translations. The local-to-moment translation, which was the most time consuming step in the original FMM algorithm, was replaced by additional operations reducing the computation time. The authors applied their code in combination with the similar subregion approach to the analysis of 2-D elastic solid containing many inclusions and to the determination of their effective elastic constants. Wang and Yao [15] presented also the FMBEM analysis of 3-D representative volume elements (RVEs) of composites modeled as elastic solids containing spherical inclusions. The efficiency of the method was further improved by parallelizing the computations (Lei et al. [5]). Liu et al. [9] applied the FMBEM to the analysis of 3-D fiber reinforced composites. The stiffeners were modeled as rigid inclusions. Thus the integral equations of elasticity was simplified. The application of the method to the analysis of carbon-nanotube composites was presented by Liu, Nishimura and Otani in [8]. Wang, Yao and Wang [19] investigated different preconditioner sparsity patterns for the iterative solution of the system of equation in the FMBEM for 2-D structures with many inclusions and cracks. The same group of authors in [14] applied the FMM to solve the traction boundary integral equation for 2-D structures containing many cracks. New preconditioner and initial vector for an effective iterative solution of the system of equations, were introduced. The application area of the method was later extended to the analysis of fatigue crack growth by Wang and Yao [18]. Zhao and Yao [22] developed a fast multipole accelerated BEM for the analysis of 3-D thin structures – plates and shells. Liu [6] presented new multipole and local expansions of 2-D linear elasticity fundamental solution in a complex form. The translations of the expansions of this formulation are exactly the same as for the 2-D potential problem case. The presented examples included analysis of plates with many circular holes. The formulation was further extended for the dual BEM, involving the traction boundary integral equation [7]. The method was applied to analysis of certain simple geometry structures, and of structures with many circular and crack-like inclusions. Ptaszny and Fedeliński [12] implemented the original FMM for the analysis of 2-D elastic structures with the use of the isoparametric quadratic boundary elements. It was shown that the discretization with the higher order elements allows to discretize structures using lower numbers of degrees of freedom (DOF), and to use expansions of lower degree in relation to the commonly used constant boundary element case. The code was further extended by the procedure of fast multipole evaluation of volume terms of the integral equation [13].

It is well known that the FMM can be applied to an efficient analysis of internal quantities, like displacements, strains and stresses. Still, there are not many examples of such analysis in the literature. Reference [20] contains stress isochromatic figures for plates with inclusions. However the authors did not mentioned by which method the stress fields were obtained. Wang and Yao [16] performed the 2-D elasto-plastic structure analysis including the FMM evaluation of the interior strains.

This work is to present authors' results of the FMBEM stress analysis of 2-D linear elastic structures. Two cases are considered: a square plate with a hole under tension, and a gear. The article is organized as follows. Section 2 contains a short introduction to the boundary element method for 2-D elastic structures. In Section 3 a basic description of the FMBEM algorithm is given. Section 4 deals with the aspects of BEM and FMBEM internal stress analysis. In section 6 a short characterization of the developed computer code is given. In Section 6 results of the internal stress analysis are presented. Section 7 contains conclusions.

2. BOUNDARY ELEMENT METHOD

An equilibrium state of a two-dimensional, statically loaded, linear elastic body Ω (Fig. 1), with boundary $\Gamma = \Gamma_1 \cup \Gamma_2$, is described by the integral equation derived from Somigliana's identity (e.g. Brebbia and Dominguez [2]):

$$C_{ij}u_j(x') + \int_{\Gamma} T_{ij}(x', x) u_j(x) d\Gamma(x) = \int_{\Gamma} U_{ij}(x', x) t_j(x) d\Gamma(x). \quad (1)$$

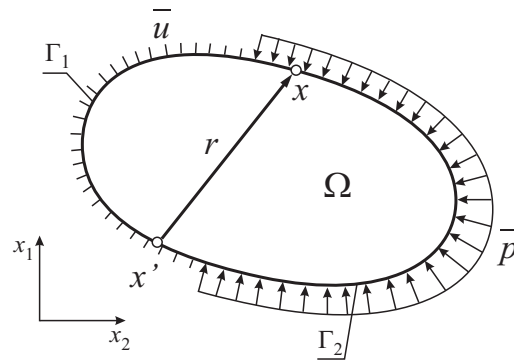


Fig. 1. Two-dimensional body Ω

In this equation u_j and t_j are displacements and tractions respectively, C_{ij} is a coefficient depending on the location of the collocation point x' , x is the integration point, and finally $T_{ij}(x', x)$ and $U_{ij}(x', x)$ are the fundamental solutions of linear elasticity:

$$U_{ij}(x', x) = \frac{1}{8\pi\mu(1-\nu)} [(4\nu - 3)\delta_{ij} \ln(r) + r_{,i}r_{,j}], \quad (2)$$

$$T_{ij}(x', x) = \frac{-1}{4\pi(1-\nu)r} \left\{ \frac{\partial r}{\partial n} [(1 - 2\nu)\delta_{ij} + 2r_{,i}r_{,j}] - (1 - 2\nu)(r_{,i}n_j - r_{,j}n_i) \right\}. \quad (3)$$

In the solutions, μ and ν are the shear modulus and Poisson's ratio respectively, n_i denotes components of the unit vector normal to the boundary and r is the distance between the collocation point and the integration point (Fig. 1). The symbol $r_{,i}$ denotes the derivative of r with respect to the i -th coordinate. The boundary of the body is discretized by using boundary elements. Equation (1) is used for each boundary node as the collocation point, boundary quantities are interpolated by using boundary element shape functions and thus a system of equations is formed. The system can be written in the matrix form:

$$[H]\{U\} = [G]\{T\}. \quad (4)$$

The matrices $[H]$ and $[G]$ depend on the fundamental solutions while $\{U\}$ and $\{T\}$ are vectors of boundary displacements and tractions. Taking into consideration boundary conditions, i.e. known displacements \bar{u} on the boundary Γ_1 , and known tractions \bar{t} on the boundary Γ_2 (Fig. 1), the system of equations can be transformed into the form:

$$[A]\{X\} = [D]\{Y\}, \quad (5)$$

where $\{X\}$ and $\{Y\}$ are vectors of the unknown and known boundary quantities. The matrices $[A]$ and $[D]$ consist of appropriate columns of the matrices $[H]$ and $[G]$. The system of equations is solved for the unknown quantities by using direct or iterative methods.

The matrices of the system of equations are fully populated and nonsymmetric. The complexity of preparation of the system is $O(N^2)$, where N is the number of boundary elements, which is proportional to the number of degrees of freedom (DOF). The properties of the system of equations make the conventional BEM inefficient in large scale analysis with respect to the computation time and required computer memory.

3. FAST MULTIPOLE BOUNDARY ELEMENT METHOD

3.1. General description of the algorithm

In this section a general idea of the fast multipole boundary element method will be introduced. For a detailed description of the method we refer the reader to the literature (e.g. [10]).

In the FMM for each collocation points near and far fields are determined. In the near field all the boundary integrals are calculated directly. In the far field expansions are used. The fields are determined by clustering of the boundary elements. The domain of the body is enclosed within a square, which is divided recursively into smaller clusters, until they contain a fixed number of boundary elements. The clusters form a hierarchical tree structure consisting of nodes, their children and ancestors, corresponding to the clusters. The clustering scheme and the tree structure are shown in Fig. 2.

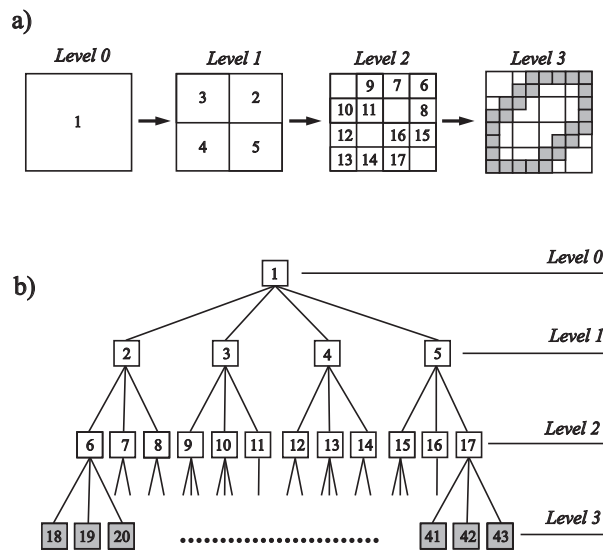


Fig. 2. (a) Clustering of the boundary elements, and (b) formation of the tree structure

The FMM uses multipole expansions of the integrals (potentials) at points located near to the integration points (Fig. 3). The expansion terms are products of multipole moments and functions. The moments depend on the locations of the expansion point and integration points, and on densities of the potentials. The functions depend on the locations of the expansion point and collocation point. Respective moments calculated for many boundary elements are added together and thus an influence of many integration points is reduced to the single point. The multipole functions are expanded further around points near to the collocation points. The series terms are products of local moments and local functions. The local moments depend on the location of the multipole and local expansion points, and are calculated by translation of the local moments (multipole-to-local translation, M2L). The local functions depend on the location of the local expansion points and the collocation points. Thus, the reduced influence is distributed to many points. The number of potential term calculations is reduced significantly in relation to the conventional BEM, where for each collocation point all the potentials coming from all integration points have to be calculated. The series of a finite number of terms are convergent when the integration points are far enough from the collocation points.

Important steps of the algorithm are translations of the multipole and local moments. The first translation is performed by shifting the multipole expansion points. The method is applied for evaluation of the moments for larger clusters, without necessity of integration along the same boundary

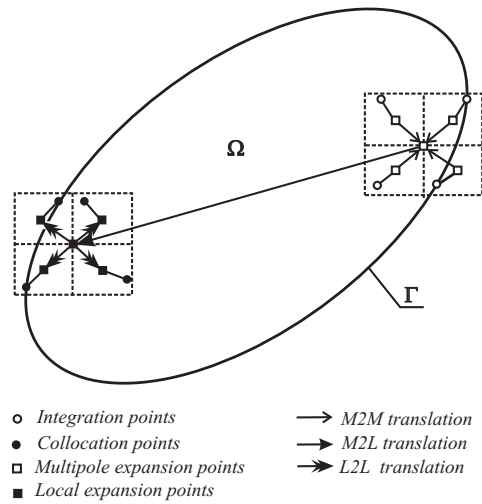


Fig. 3. General scheme of the fast multipole method

elements and internal cells. The operation is called multipole-to-multipole (M2M) translation. Similarly the local moments are transformed by shifting the local expansion point. Thus, new moments for smaller clusters are calculated which are applied to the evaluation of the far-field terms of the potentials. As the result of all the operations, products of the matrices and the boundary quantities vectors are obtained and elements of the volume potential vector as well. Summarizing, the algorithm consists of the following steps:

- Clustering of the boundary elements.
- Calculation of the multipole moments for leaves of the tree (the smallest clusters).
- Multipole-to-multipole (M2M) translation of the moments.
- Multipole-to-local (M2L) translation.
- Local-to-local (L2L) translation.
- Evaluation of the potential terms by using the local expansion of leaves.

Figure 4 shows the sequence of translations of the moments.

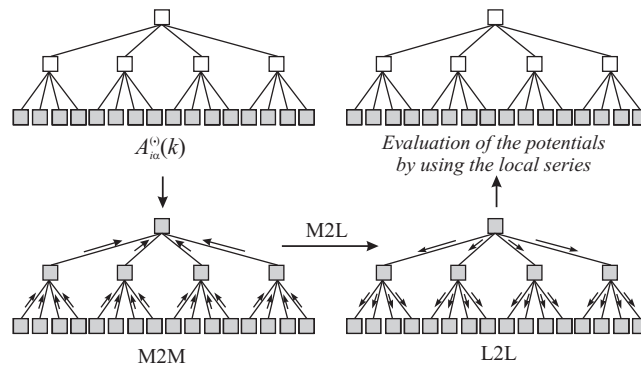


Fig. 4. Translations of the multipole and local moments

The system of equations (5) can now be written in the following form:

$$[A]^{near} \{X\} + \{AX\}^{far} = [D]^{near} \{Y\} + \{DY\}^{far}. \tag{6}$$

The 'near' matrices and vectors include the near field terms of the potentials calculated directly, whilst the 'far' ones correspond to the far-field influence, coming from so-called interaction sets of clusters, and are computed by using expansions. The system of equations can be solved only by using an iterative solver as the matrices are not calculated explicitly. The complexity of the method is $O(N)$.

3.2. Multipole and local series of the potentials

In Eq. (1) the integrals are:

- single layer potential:

$$\sum_j I_{ij}^U(x') = \int_{\Gamma} U_{ij}(x', x) t_j(x) d\Gamma(x), \quad x' \in \Omega, \quad x \in \Gamma, \quad (7)$$

- double layer potential:

$$\sum_j I_{ij}^T(x') = \int_{\Gamma} T_{ij}(x', x) u_j(x) d\Gamma(x), \quad x' \in \Omega, \quad x \in \Gamma. \quad (8)$$

In the multipole methods the far-field potentials are expanded into a series around a point close to the integration points. An expansion of a single term of the single layer potential around the point c (Fig. 5) will be considered. The term corresponds to the influence of integration points located at boundary elements β clustered in the cluster α .

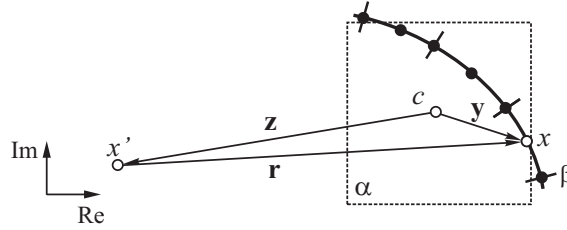


Fig. 5. Scheme of the multipole expansion

By using the formulation given in [21] the series can be written as:

$$I_{11\alpha}^U(x') = \frac{1}{8\pi\mu(1-\nu)} \operatorname{Re} \sum_{k=0}^{\infty} [(4\nu-3) A_{1\alpha}^0(k) f(\mathbf{z}, k) + A_{1\alpha}(k) f^{Re}(\mathbf{z}, k+1) - A_{1\alpha}^{Re}(k) f(\mathbf{z}, k+1)], \quad (9)$$

with the multipole moments:

$$A_{i\alpha}(k) = \sum_{\beta} \int_{\Gamma_{\beta}} \mathbf{y}^k t_{i\beta} d\Gamma(x), \quad (10)$$

$$A_{i\alpha}^{Re}(k) = \sum_{\beta} \int_{\Gamma_{\beta}} \operatorname{Re} \mathbf{y}^k t_{i\beta} d\Gamma(x), \quad (11)$$

for $k = 0, 1, \dots, \infty$; and

$$A_{i\alpha}^0(k) = \begin{cases} A_{i\alpha}(k) & \text{for } k = 0, \\ -\frac{1}{k} A_{i\alpha}(k) & \text{for } k = 1, 2, \dots, \infty. \end{cases} \quad (12)$$

We assume that the expansions are convergent if

$$|\mathbf{y}| \leq \frac{1}{2}|\mathbf{z}|. \quad (13)$$

The vectors \mathbf{y} and \mathbf{z} connect the expansion point c to the integration point x , and the expansion point c to the collocation point x' respectively (Fig. 5). The multipole functions are:

$$f(\mathbf{z}, k) = \begin{cases} \ln \mathbf{z} & \text{for } k = 0, \\ \mathbf{z}^{-k} & \text{for } k = 1, 2, \dots, \infty. \end{cases} \quad (14)$$

$$f^{Re}(\mathbf{z}, k) = \text{Re } \mathbf{z} \mathbf{z}^{-k}. \quad (15)$$

The multipole moments, which include the influence of the integration points, are transformed by the translation of the expansion point (M2M translation). Appropriate formulas can be found in the literature (e.g. [1, 20]). Next, the M2L translation is performed resulting in the local series (Fig. 6):

$$I_{11\alpha}^U(x') = \frac{1}{8\pi\mu(1-\nu)} \text{Re} \sum_{k=0}^{\infty} [(4\nu - 3)E_{1\alpha'}^0(\alpha, k)g(\mathbf{y}', k) + E_{1\alpha'}^{Re}(\alpha, k)g(\mathbf{y}', k) - E_{1\alpha'}(\alpha, k)g^{Re}(\mathbf{y}', k)] \quad (16)$$

for

$$|\mathbf{y}'| \leq \frac{1}{2}|\mathbf{z}'|. \quad (17)$$

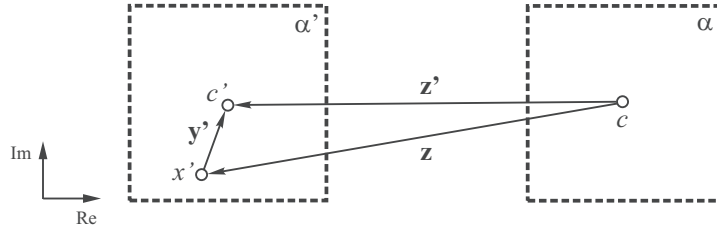


Fig. 6. Scheme of the local expansion

The local moments are obtained by the application of the M2L formulas:

$$E_{i\alpha'}^0(\alpha, l) = \begin{cases} \ln \mathbf{z}' A_{i\alpha}^0(0) + \sum_{k=1}^{\infty} \binom{l+k-1}{k-1} (\mathbf{z}')^{-k-l} A_{i\alpha}(k), & \text{for } l = 0, \\ -\frac{1}{l} (\mathbf{z}')^{-l} A_{i\alpha}^0(0) + \sum_{k=1}^{\infty} \binom{l+k-1}{k-1} (\mathbf{z}')^{-k-l} A_{i\alpha}(k) & \text{for } l = 1, 2, \dots, \infty, \end{cases} \quad (18)$$

$$E_{i\alpha'}(\alpha, l) = \sum_{k=0}^{\infty} \binom{l+k}{k} (\mathbf{z}')^{-k-l-1} A_{i\alpha}(k), \quad (19)$$

$$E_{i\alpha'}^{Re}(\alpha, l) = \sum_{k=0}^{\infty} \binom{l+k}{k} (\mathbf{z}')^{-k-l-1} \left[\text{Re } \mathbf{z}' A_{i\alpha}(k) - A_{i\alpha}^{Re}(k) \right], \quad (20)$$

The local functions are defined as follows:

$$g(\mathbf{y}', k) = (\mathbf{y}')^k, \quad (21)$$

$$g^{Re}(\mathbf{y}', k) = (\mathbf{y}')^k \text{Re } \mathbf{y}'. \quad (22)$$

The translation was constructed by application of the following expansions:

$$\ln(\mathbf{z}' - \mathbf{y}') = \ln \mathbf{z}' + \sum_{l=1}^{\infty} \frac{-1}{l} \left(\frac{\mathbf{y}'}{\mathbf{z}'} \right)^l, \quad (23)$$

$$(\mathbf{z}' - \mathbf{y}')^{-k} = (\mathbf{z}')^{-k} \sum_{l=0}^{\infty} \binom{l+k-1}{k-1} \left(\frac{\mathbf{y}'}{\mathbf{z}'} \right)^l, \quad (24)$$

with the condition (17) satisfied.

4. CALCULATION OF STRESSES

Somigliana's identity can be applied to the evaluation of displacements at any point of the body Ω , when all boundary displacements and tractions are known. A stress integral equation can be obtained by the differentiation of equation (1) with respect to x' , and applying the strain-displacement and the stress-strain relationships. The stress integral equation has the form:

$$\sigma_{ij}(x') = \int_{\Gamma} U_{ijk}(x', x) t_k(x) d\Gamma(x) - \int_{\Gamma} T_{ijk}(x', x) u_k(x) d\Gamma(x). \quad (25)$$

The new fundamental solutions are:

$$U_{ijk}(x', x) = \frac{1}{4\pi(1-\nu)r} [2r_{,i}r_{,j}r_{,k} + (1-2\nu)(\delta_{kj}r_{,i} + \delta_{ki}r_{,j} - \delta_{ij}r_{,k})], \quad (26)$$

$$T_{ijk}(x', x) = \frac{2\mu}{4\pi(1-\nu)r^2} \left\{ 2 \frac{\partial r}{\partial n} [(1-2\nu)\delta_{ij}r_{,k} + \nu(\delta_{jk}r_{,i} + \delta_{ki}r_{,j}) - 4r_{,i}r_{,j}r_{,k}] \right. \\ \left. + 2\nu(n_i r_{,j}r_{,k} + n_j r_{,k}r_{,i}) + (1-2\nu)(\delta_{kj}n_i + \delta_{ki}n_j + 2r_{,i}r_{,j}n_k) - (1-4\nu)\delta_{ij}n_k \right\}. \quad (27)$$

By using this equation one can calculate stress components at any point of the body.

The boundary stress components are usually evaluated by means of the boundary quantities. The derivatives of shape functions are used to calculate strain components. The boundary strains and traction forces allow to calculate all boundary stress components. This method is convenient due to reduced computation time in comparison with the application of the stress integral equation. However stress evaluation at internal points requires the usage of the stress integral equation, which can result in a significant time cost in the case of a large number of the internal points, due to time consuming integration operations. In order to reduce the computation time one can apply the FMM, which requires an expansion of the potentials.

The direct expansion of the fundamental solutions (26) and (27) is complicated as the formulas have relatively complex form. Therefore a common choice for the derivation of expansions of the potentials occurring in the equation (25) is the transformation of the expansions built for the displacement-equation potentials. For example, by taking the derivative of the potential (7) with respect to the j -th coordinate of x' one can obtain:

$$\frac{\partial}{\partial x'_j} \left\{ \sum_{\beta} \int_{\Gamma_{\beta}} U_{ik}(x', x) t_{k\beta} d\Gamma(x) \right\} = - \sum_k I_{ik\alpha,j}^U(x'). \quad (28)$$

A new potential is introduced:

$$I_{ijk\alpha}^U(x') = I_{ik\alpha,j}^U(x'), \quad (29)$$

which can be calculated by using the expansion (16), with the local functions replaced by their derivatives. For a single term we have:

$$I_{1j1\alpha}^U(x') = \frac{1}{8\pi\mu(1-\nu)} \operatorname{Re} \sum_{k=0}^{\infty} [(4\nu-3)E_{1\alpha'}^0(k)g_{,j}(\mathbf{y}',k) + E_{1\alpha'}^{Re}(k)g_{,j}(\mathbf{y}',k) - E_{1\alpha'}(k)g_{,j}^{Re}(\mathbf{y}',k)], \quad (30)$$

with the derivatives of the local functions:

$$g_{,j}(\mathbf{y}',k) = k(\mathbf{y}')^{k-1} \left\{ \begin{array}{c} 1 \\ i \end{array} \right\}, \quad (31)$$

$$g_{,j}^{Re}(\mathbf{y}',k) = k(\mathbf{y}')^{k-1} \operatorname{Re}(\mathbf{y}') \left\{ \begin{array}{c} 1 \\ 0 \end{array} \right\} + (\mathbf{y}')^k \left\{ \begin{array}{c} 1 \\ i \end{array} \right\}, \quad (32)$$

where $i = \sqrt{-1}$. The term of the stress integral equation can be calculated by the application of the constitutive equation:

$$\sum_{\beta} \int_{\Gamma_{\beta}} U_{ijk}(x',x) t_{k\beta} d\Gamma(x) = \sum_k \left\{ \frac{2\mu\nu}{1-2\nu} \delta_{ij} I_{llk\alpha}^U(x') + \mu [I_{ijk\alpha}^U(x') + I_{jik\alpha}^U(x')] \right\}. \quad (33)$$

Consequently all the far-field terms of the stress equation potentials can be obtained. Summarizing, the stress calculations can be performed by using the same multipole and local moments and their translations as for the displacement equation potentials. The calculations are performed as a post process step, after the system of equation (4) or (5) is solved and all boundary displacements and tractions are known.

In order to recover the stress field within the area of the structure or its part internal points have to be determined. The points can be nodes of cells which can be applied to the interpolation of the analyzed field. The internal points are treated as collocation points and for each of them the equation (25) is applied. The points have to be clustered and assigned to appropriate nodes of the tree. Assuming that the points are nodes of cells, the clustering of cells has to be performed (Fig. 7).

The complexity of the internal stress evaluation stage is $O(N+M)$, where N is the number of boundary elements, proportional to the number of DOF, and M is the number of cells which is proportional to the number of internal points.

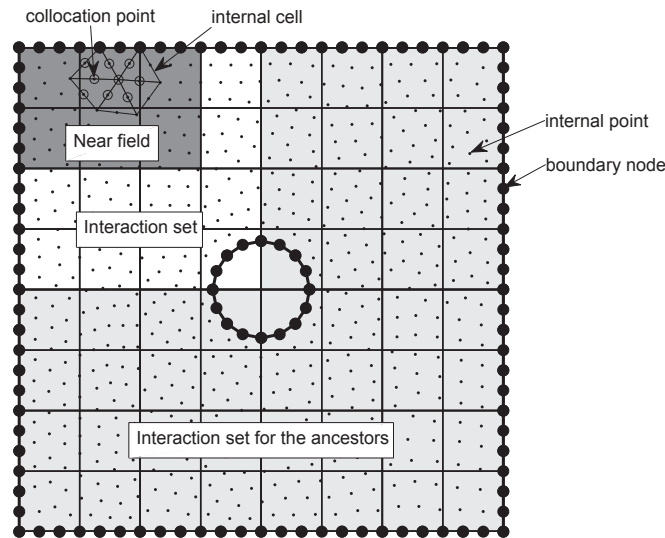


Fig. 7. Clustering of the boundary elements and cells with internal points

5. COMPUTER CODE

A FMBEM code for the stress analysis of elastic plates loaded statically is developed [12]. The boundary of structure is discretized using three-node quadratic boundary elements and the domain is discretized using six-node internal cells. The regular boundary integrals are calculated using the Gauss quadrature. The singular boundary integrals are calculated using logarithmic Gauss quadrature or rigid body movement method, respectively. The system of equations is solved by using the preconditioned GMRES. The preconditioner sparsity pattern based on leaves of the tree was used. In the case of the internal stress analysis the cell nodes determine internal points, and the cells are used for the interpolation of the analyzed field.

6. NUMERICAL EXAMPLES

6.1. Square plate with a hole

In this example stresses in the whole area of a quadratic plate with a circular hole were analyzed. The plate is loaded by tensile forces, as it is shown in the Fig. 8. The side length is $a = 1$ m and the hole radius is $r = 0.1$ m. The traction force value is $p = 100$ MPa. The material properties are as follows: Young's modulus $E = 200$ GPa and Poisson's ratio $\nu = 0.3$. The plate is in plane stress. Three discretization cases were considered as it is shown in Fig. 9 and Table 1. The same structure were analysed by Liu [6] and by Ptaszny and Fedeliński [12]. In the cited articles only boundary stresses were analyzed.

The boundary stress was calculated by using the boundary quantities, evaluated by the conventional BEM. The internal stress was evaluated at internal points by the BEM or the FMBEM (we will refer to the last scheme as BEM/FMBEM). The points were used as cell-nodes for the visual-

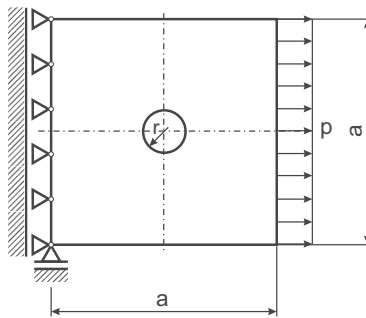


Fig. 8. Quadratic plate with a circular hole

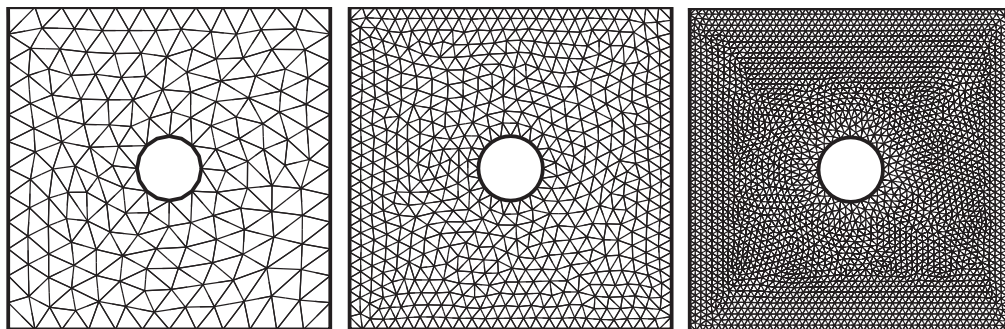


Fig. 9. Three models of the plate

Table 1. Parameters of the plate numerical models

| Model No. | Number of boundary elements | Number of internal points |
|-----------|-----------------------------|---------------------------|
| 1 | 56 | 592 |
| 2 | 120 | 2220 |
| 3 | 220 | 10672 |

ization the stress distribution and calculation of the elastic energy of the structure. The maximum number of cells in a leaf was equal to 20. Series of $w = 5, 10$ and 15 terms were applied.

As a result of the analysis a distribution of stress within the whole structure area was obtained. Figure 10 shows the reduced Huber-Mises stress distribution maps for the finest discretization case. For the verification of the results the elastic energy of the structure was computed as follows:

$$U = \frac{1}{2} \int_{\Omega} \sigma^T E \sigma \, d\Omega, \tag{34}$$

where Ω is the domain of the structure, σ is the matrix of stress components and E is the matrix of the material elastic coefficients. A relative difference of the energy was calculated:

$$\varepsilon = \frac{||U_3^{\text{BEM}}|| - ||U||}{||U_3^{\text{BEM}}||} \cdot 100\%, \tag{35}$$

with respect to the energy norm obtained by the BEM for the finest model:

$$||U_3^{\text{BEM}}|| = \sqrt{U_3^{\text{BEM}}}. \tag{36}$$

The elastic energy values obtained by using different methods are shown in Table 2 and Fig. 11. The values of the relative difference obtained by the BEM and the BEM/FMBEM for all the models and different numbers of expansion terms are shown in Table 3.

In the case of the BEM/FMBEM analysis with 5 expansion terms the resulting stresses were the most different from the ones calculated by the BEM. Analyzing the stress plots, Fig. 10, one can see local stress discontinuities. They are more visible with growing number of internal points and caused by the truncation error. When at least 10 terms are used the stress field is continuous. The energy value (Table 2, Fig. 11) and the relative difference value (Table 3) confirm the lower accuracy of the 5-termed expansion analysis results. For such number of terms the energy converges to a different value from that observed in the case of the BEM analysis. This means that the truncation error exceeds the discretization error. For both cases of 10 and 15 terms the truncation error gets lower as the number of internal points grows. For all the cases the relative difference does not exceed 0.15%.

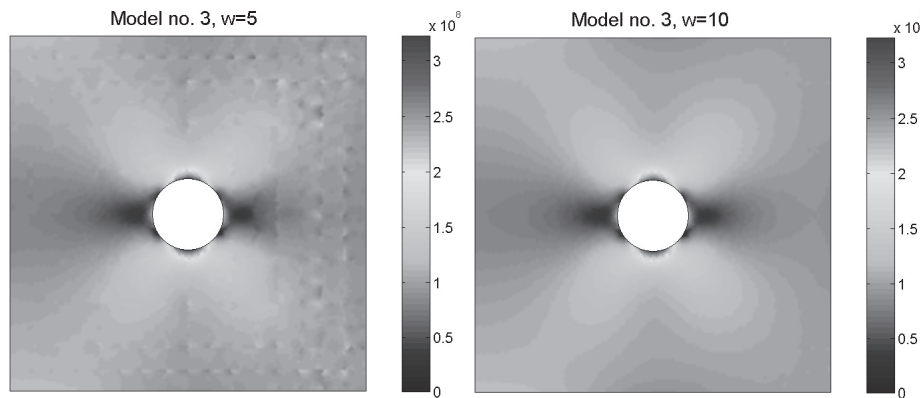


Fig. 10. Huber-Mises stress distribution plots

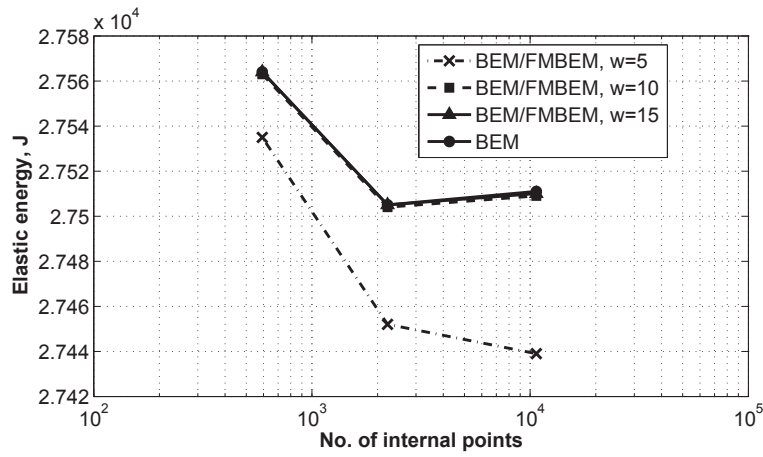


Fig. 11. Elastic energy calculated by the BEM and the BEM/FMBEM

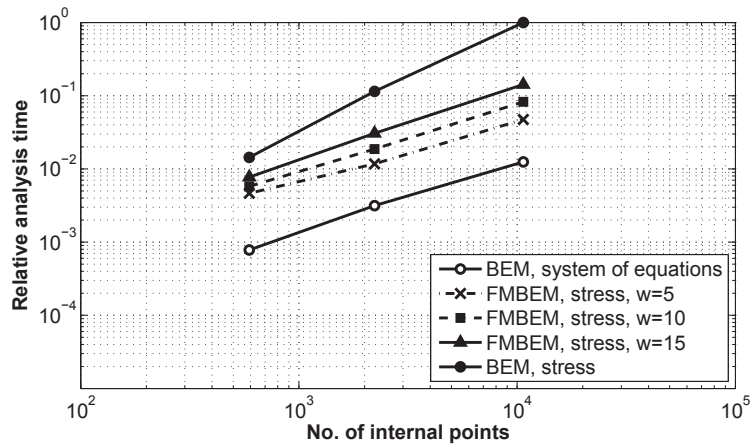


Fig. 12. BEM and BEM/FMBEM relative analysis time

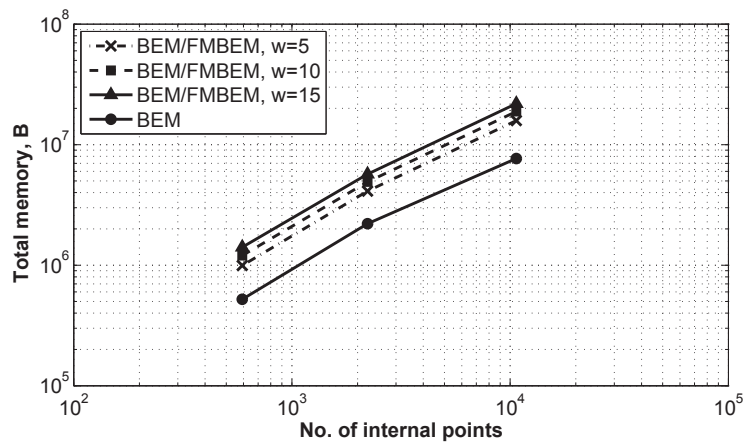


Fig. 13. BEM and BEM/FMBEM memory

Table 2. Elastic energy calculated by the BEM and the BEM/FMBEM

| Model No. | U [J] | | | |
|-----------|-----------|-----------|----------|----------|
| | MEB (BEM) | BEM/FMBEM | | |
| | | $w = 5$ | $w = 10$ | $w = 15$ |
| 1 | 27 564 | 27 535 | 27 563 | 27 564 |
| 2 | 27 505 | 27 452 | 27 504 | 27 505 |
| 3 | 27 511 | 27 439 | 27 509 | 27 510 |

Table 3. Relative difference of the elastic energy calculated by using the BEM/FMBEM

| Model No. | ε [%] | | |
|-----------|-------------------|----------|----------|
| | $w = 5$ | $w = 10$ | $w = 15$ |
| 1 | -0.044 | -0.096 | -0.097 |
| 2 | 0.106 | 0.012 | 0.010 |
| 3 | 0.130 | 0.004 | 0.002 |

When the expansion degree is at least 10 the BEM/FMBEM results agree with the BEM ones, and the relative difference error tends to a value of order of 0.01%.

Internal stress analysis time was investigated. Figure 12 shows a normalized stress computation time, and the time of solution of the system of equations, related to the BEM stress calculation time for the largest number of internal points. The stress calculation time has a significant influence on the overall computation time, as it is by almost 100 times longer than the time of the BEM solution of the system of equations. The analysis time can be shortened by over 5 times using the FMBEM with 15 expansion terms, by 10 times for 10 expansion terms, or even by 15 times when 5 expansion terms are used (Fig. 12). The FMBEM analysis time grows less intensely than the BEM one, with growing number of internal points.

Required memory was also investigated. A comparison of memory for different methods is shown in Fig. 13. In the case of the BEM/FMBEM analysis the memory is larger than for the BEM. In all the cases for the evaluation of the boundary values the conventional BEM with fully populated matrices was used. The FMBEM requires also a storage of the clustering tree structure, with multipole and local moments.

6.2. Gear

Displacements and stresses in a gear of the involute tooth profile were analyzed. The geometry of the gear is shown in Fig. 14. The dimensions are given in millimeters. The tooth profile parameters are shown in Table 4. It is assumed that the number of teeth of the mating gear is 80. The axes of both gears are located on a vertical plane, and the mating gear is located above the analyzed one. The gears are in position corresponding to the interaction of a single teeth couple. The circumferential force acting at the contact point of pitch cylinders $F_o = 2670$ N. It was assumed that a single tooth

Table 4. Parameters of the gear tooth

| Parameter | Value |
|---------------------------|--------|
| No. of teeth | 40 |
| Module | 2 mm |
| Angle of action | 20° |
| Pitch diameter | 80 mm |
| Addendum | 4.5 mm |
| Tooth depth fillet radius | 0.4 mm |

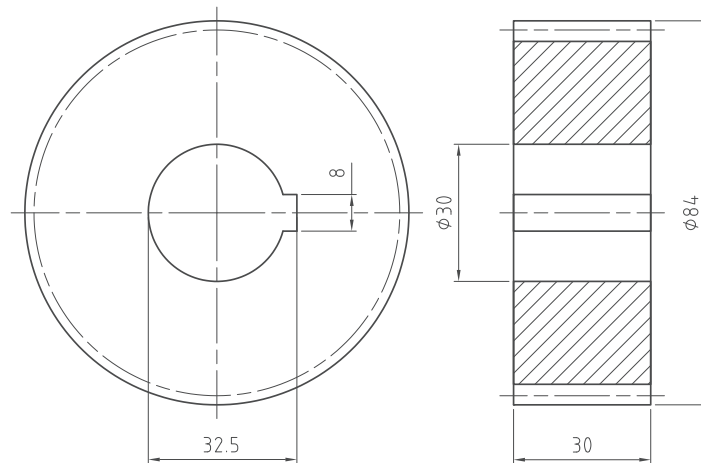


Fig. 14. Gear geometry

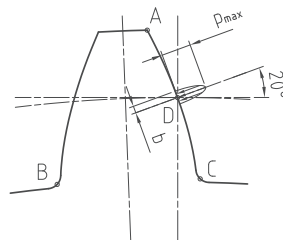


Fig. 15. Tooth load scheme

is loaded by a traction force of distribution described by the Hertz theorem for two interacting cylinders of radii dependent on the pitch diameters and the angle of action, as it is commonly assumed in engineering calculations of gears. The load parameters (Fig. 15) are: $p_{\max} = 602.7$ MPa and $b = 0.1$ mm. The inner boundary of the model was clamped. The gear material is steel of the parameters: Young's modulus $E = 200$ GPa and Poisson ratio $\nu = 0.3$. The model is in plane strain.

The outer boundary was divided into 2688 quadratic boundary element, each of the length approximately equal to $2b$. The number of DOF was equal to 10752. Such discretization scheme allowed to model the load along a single element. The area of the loaded tooth was divided into cells (Fig. 16).

At the cell node stresses were calculated and the cells were used to visualize the stress field. The parameters of the BEM model are listed in Table 5.

Table 5. Parameters of the BEM model

| No. | Value |
|--------------------|-------|
| Boundary elements | 2688 |
| Internal points | 1099 |
| Internal cells | 572 |
| Degrees of freedom | 10752 |

The number of DOF is too large for an effective analysis by using the conventional BEM. The FMBEM analysis was performed by using sequantly $w = 5$ and 10 expansion terms. The preconditioner sparsity pattern was based on leaves of the tree. The maximum allowed number of cells in a leaf was set to 250. The relative tolerance for the GMRES iterative solver was set to 10^{-6} .

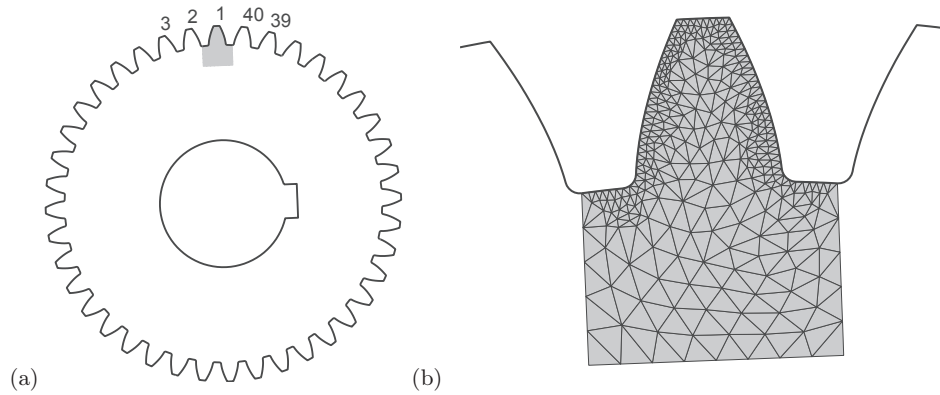


Fig. 16. Geometry of the BEM model: (a) the tooth numbering, (b) the discretized region

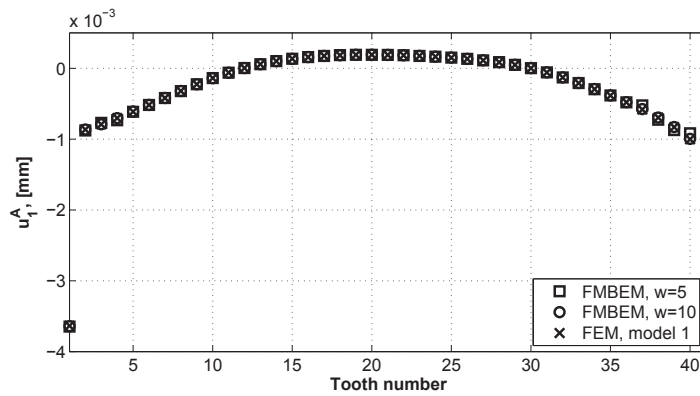


Fig. 17. Tooth vertice horizontal displacement

The FMBEM analysis results were compared with other results obtained by the MSC Patran/Nastran commercial FEM software. Two FEM model were developed:

1. A model of the whole gear with the same boundary node distribution as in the BEM model. The boundary condition were the same as for the BEM model.
2. A model of a single tooth according to the discretized area of the BEM model. The number of the boundary nodes at the tooth-profile boundary was by 10 times larges than for the first model. The model was clamped at the artificial boundary, dividing the tooth from the remaining part of the gear.

Both the FEM models were discretized by using six-node triangle elements with quadratic shape functions. All parameters of the considered models are shown in Tables 5 and 6, respectively.

Table 6. Parameters of the FEM models

| No. | Model | No. of elements | No. of DOF |
|-----|--------------|-----------------|------------|
| 1 | Whole gear | 28 278 | 118 008 |
| 2 | Single tooth | 14 831 | 15 646 |

Displacements of the vertice A of the first tooth (Fig. 15) and corresponding vertices of the remaining teeth were analyzed. The tooth numbering is shown in Fig. 16(a). Figures 17 and 18 show a comparison of the horizontal and vertical displacements respectively, obtained by the FMBEM

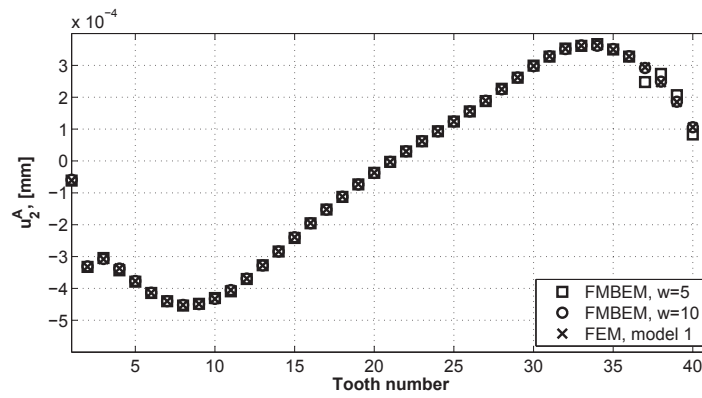


Fig. 18. Tooth vertex vertical displacement

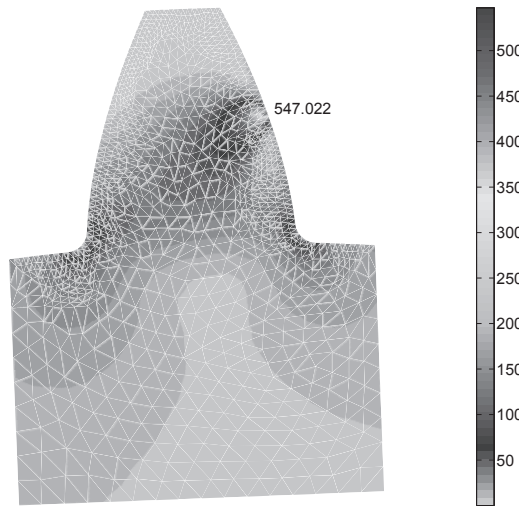


Fig. 19. Distribution of Huber-Mises stress (MPa) calculated by using the FMBEM

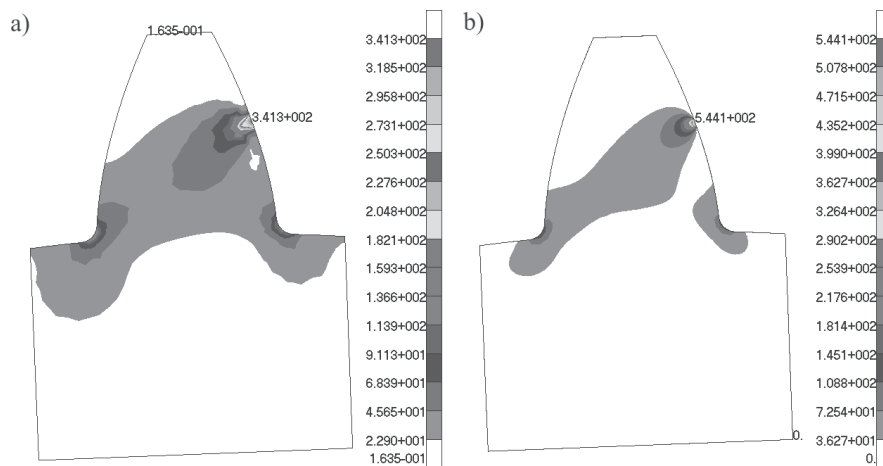


Fig. 20. Distribution of the reduced Huber-Mises stress (MPa) calculated using the FEM: (a) for the model 1, (b) for the model 2

for $w = 5$ and 10 expansion terms, and by the FEM for the 1st model. The number of terms does not influence significantly the FMBEM results which agree with the FEM ones.

The reduced Huber-Mises stress distribution within the loaded tooth area was investigated. For the internal stress calculation 10 expansion terms were used, independently on the expansion degree used for the boundary quantities evaluation. The results obtained by using 5 terms of expansion for the boundary quantities evaluation are shown in Fig. 19. The results obtained by the FEM for the two considered models are shown in Fig. 20.

The Huber-Mises stress at the points B, C and D of the 1st tooth profile, where a stress concentration occurs, was evaluated. A comparison of the values computed by using different methods are listed in Table 7. The FEM analysis results for the 1st model are underrated in comparison with the 2nd FEM model and the FMBEM results, which are consistent (Table 7). The 2nd FEM model was discretized with a more dense finite element mesh than the 1st model. It can be concluded, that the FMBEM gives more accurate results than the FEM with the same node density at the boundary.

Table 7. Maximal Huber-Mises stress at the points B, C and D

| Method | Reduced stress (MPa) at the point | | |
|-----------------|-----------------------------------|-------|-------|
| | B | C | D |
| FMBEM, $w = 5$ | 160.2 | 137.3 | 547.0 |
| FMBEM, $w = 10$ | 160.4 | 137.4 | 547.0 |
| FEM, model 1 | 152.6 | 130.3 | 341.3 |
| FEM, model 2 | 157.4 | 137.1 | 544.1 |

7. CONCLUSIONS

In this paper the FMBEM analysis of internal stress in 2-D linear elastic structures was presented. The boundary stress was calculated by the differentiation of the boundary element shape functions and application of the strain-displacement and stress-strain relations. For the evaluation of internal stress series were applied. The series of the stress integral equation potentials were obtained by differentiation of the local functions of displacement equation potentials, and subsequent application of the same relations as in the case of the boundary stress. In the numerical example a structure with stress concentration was considered. Accuracy, analysis time and required memory were investigated. The elastic energy of analyzed structure can be evaluated with accuracy of order of 0.1% or better, when 5 or more expansion terms are used for the internal stress analysis. It was shown, that the analysis time can be reduced in relation to the conventional BEM analysis, for structures with relatively small number of degrees of freedom, when the number of internal points is of order of 10^2 and larger.

REFERENCES

- [1] R. Beatson, L. Greengard. A short course on fast multipole methods. <http://www.math.nyu.edu/faculty/greengar/>
- [2] C.A. Brebbia, J. Dominguez. *Boundary elements an introductory course*. McGraw-Hill, New York, 1992.
- [3] J. Englund, J. Helsing. Stress computations on perforated polygonal domains. *Eng. Anal. Bound. Elem.*, **27**: 533-546, 2003.
- [4] L. Greengard, V. Rokhlin. A fast algorithm for particle simulations. *J. Comput. Phys.*, **73**: 325-348, 1987.
- [5] T. Lei, Z. Yao, H. Wang, P. Wang. A parallel fast multipole BEM and its applications to large-scale analysis of 3-D fiber-reinforced composites. *Acta Mech. Sinica*, **22**: 225-232, 2006.
- [6] Y.J. Liu. A new fast multipole boundary element method for solving large-scale two-dimensional elastostatic problems. *Int. J. Numer. Meth. Engng.*, **65**: 863-881, 2006.
- [7] Y.J. Liu. A fast multipole boundary element method for 2D multi-domain elastostatic problems based on a dual BIE formulation. *Comput. Mech.*, **42**: 761-773, 2008.

- [8] Y.J. Liu, N. Nishimura, Y. Otani. Large-scale modeling of carbon-nanotube composites by a fast multipole boundary element method. *Comput. Mater. Sci.*, **34**: 173-187, 2005.
- [9] Y.J. Liu, N. Nishimura, Y. Otani, T. Takahashi, X.L. Chen, H. Munakata. A fast boundary element method for the analysis of fiber-reinforced composites based on a rigid-inclusion model. *J. Appl. Mech.*, **72**: 115-128, 2005.
- [10] N. Nishimura. Fast multipole accelerated boundary integral equation methods. *Appl. Mech. Rev.*, **55**: 299-324, 2002.
- [11] G. Of, O. Steinbach, W.L. Wendland. Applications of a fast multipole Galerkin boundary element method in linear elastostatics. *Bericht 2004/09, SFB 404*, Universität Stuttgart, 2004.
- [12] J. Ptaszny, P. Fedeliński. Fast multipole boundary element method for the analysis of plates with many holes. *Arch. Mech.*, **59**: 385-401, 2007.
- [13] J. Ptaszny, P. Fedeliński. Fast multipole boundary element method in analysis of structures loaded by volume forces (in Polish). *Engineering Modeling*, **35**: 107-114, 2008.
- [14] H. Wang, Z. Yao, P. Wang. On the preconditioners for fast multipole boundary element methods for 2D multi-domain elastostatics. *Eng. Anal. Bound. Elem.*, **29**: 673-688, 2005.
- [15] H.T. Wang, Z.H. Yao. A new fast multipole boundary element method for large scale analysis of mechanical properties in 3D particle-reinforced composites. *CMES - Comp. Model. Eng.*, **7**: 85-95, 2005.
- [16] P.B. Wang, Z.H. Yao, Fast multipole boundary element analysis of two-dimensional elastoplastic problems. *Commun. Numer. Meth. Engng.*, **23**: 889-903, 2007.
- [17] P.B. Wang, Z.H. Yao. Application of a new fast multipole BEM for simulation of 2D elastic solid with large number of inclusions. *Acta Mech. Sinica*, **20**: 613-622, 2004.
- [18] P.B. Wang, Z.H. Yao. Fast multipole DBEM analysis of fatigue crack growth. *Comput. Mech.*, **38**: 223-233, 2006.
- [19] P. Wang, Z. Yao, H. Wang. Fast multipole BEM for simulations of 2-D solids containing large number of cracks. *Tsingua Science and Technology*, **10**: 76-81, 2005.
- [20] Z. Yao, F. Kong, H. Wang, P. Wang. 2D simulation of composite materials using BEM. *Eng. Anal. Bound. Elem.*, **28**: 927-935, 2004.
- [21] Y. Yamada, K. Hayami. A multipole boundary element method for two dimensional elastostatics, *Tech. Rep., METR 95-07*, Math. Eng. Section, Dept. Math. Eng., Information Phys., Univ. Tokyo, 1995.
- [22] L. Zhao, Z. Yao. Fast multipole BEM for 3-D elastostatic problems with applications for thin structures. *Tsingua Science and Technology*, **10**: 67-75, 2005.